Chemical Physics 375 (2010) 348–358

Contents lists available at ScienceDirect

Chemical Physics

journal homepage: www.elsevier.com/locate/chemphys

Intrinsic common noise in a system of two coupled Brusselators

Amitabha Nandi, Benjamin Lindner *

Max-Planck Institut für Physik komplexer Systeme, Nöthnitzer Str. 38, 01187 Dresden, Germany

ARTICLE INFO

Article history:
Received 18 January 2010
In final form 9 March 2010
Available online 15 March 2010

This paper is devoted to P. Hänggi on occasion of his 60th birthday

Keywords:
Correlation
Stochasticity
Intrinsic coupling
Common noise
Brusselator
Stochastic limit cycle

ABSTRACT

We investigate effects of coupling two chemical subsystems through diffusion of chemical species. We consider the Langevin description of the actual microscopic dynamics and show that diffusive coupling gives rise to a common noise term along with the deterministic interaction. As a model example, we study two diffusively coupled Brusselator systems. By numerical Langevin simulations, we inspect the effect of the common noise term on the total correlation between the two Brusselators; we also verify the validity of the Langevin approach by comparison to simulations of the more accurate master equation. The intrinsic common noise has its strongest effect for the Brusselator dynamics operating at a stable fixed point far from the Hopf bifurcation; in this case, the common noise reduces the correlation of the Brusselators significantly. We also show that for specific parameter sets the covariance between the systems is maximized (or minimized) at a finite system size.

1. Introduction

Intrinsic noise is important in chemical reactions that involve only a small number of molecules. This condition is met in many biochemical reactions that occur in cells [1] which are additionally subject to environmental (external) noise [1,2]. Dynamical behaviors that are shaped by these noise sources range from mere steady-state fluctuations [2] to sustained stochastic oscillations [3–6] and transitions between metastable states [7].

Effects of intrinsic noise can be either studied by the master equation for the actual number of reacting molecules [8] or by the chemical Langevin equation (CLE) and its corresponding Fokker–Planck equation [9,10]; the limitations of the latter have been explored by Peter Hänggi in his early work, see, e.g. [11,12]. The CLE basically represents a stochastic version of the well-known rate equations of chemical physics. Therefore, in many cases it is more instructive than the master equation because in the deterministic limit (infinitely many molecules), the CLEs correspond to the standard rate equations. For example, if the rate equations show a limit-cycle solution, it is plausible from the respective Langevin equations that the corresponding finite system displays stochastic oscillations. This behavior would be much harder to predict from the more exact but cumbersome master equation. Numerical studies have shown that the Langevin equation can approximate the master equation faithfully for sufficiently high number of molecules [10].

The description by a master equation becomes particularly cumbersome for *coupled* chemical systems. Such systems are of special interest because they are capable of *cooperative* behavior. In order to theoretically describe phenomena like synchronization, which are ubiquitous in a wide variety of natural systems [13], coupled rate or Langevin equations are often considered instead of the full master equation (for limitations of the rate-equation approach compared to the master equation in a coupled system, see Ref. [14]). Such mathematical models can describe, for instance, cooperative behavior in coupled biochemical systems, observed across a large population of cells [15,16,4,17–19]. Here, intercell signaling provides the dynamical coupling, for instance, by quorum sensing [20,21] (signaling molecules exchanged between cells regulating their behavior).

Distributed systems can show strong correlations even if its elements are uncoupled but all elements are driven by a common stimulus. This has been studied in detail, for generic limit-cycle oscillators [22,23] and for excitable neural models [24] as well as experimentally in real neurons [25,26].

In this paper we are interested in the effects of intrinsic common noise arising from the coupling of chemical systems. From a theoretical point of view, this brings together the two different origins of cooperative behavior emerging in distributed systems: coupling and common stimulus. As an example, consider two subsystems specified by variables $\{\mathbf{X}\}$ and $\{\mathbf{X}'\}$ and having similar reaction channels. Assume that there is one chemical species, say

* Corresponding author.
E-mail address: benji@pks.mpg.de (B. Lindner).

0301-0104/$ - see front matter © 2010 Elsevier B.V. All rights reserved.
doi:10.1016/j.chemphys.2010.03.006

X_i and X_i' which can freely diffuse between them [27]. The corresponding reaction channels

$$X_i \underset{\varepsilon'}{\overset{\varepsilon}{\rightleftharpoons}} X_i', \tag{1}$$

couple the two subsystems. Depending on the rate of diffusion governed by ε and ε', the other variables X_j and X_j' (with $j \neq i$) can display correlations. As we will argue in the next section, such coupling via Eq. (1) introduces besides the usually considered deterministic interaction term, a common noise term in the chemical Langevin equation for the coupled system. The specific form of the common noise is multiplicative (it involves the number of molecules of the diffusing species) and anti-correlated between the systems (it enters with different signs into the dynamics of the two subsystems). In order to separate out the effects of the deterministic coupling and the common noise, we artificially set one of them to zero and compare the resulting correlation statistics to those of the full system. We also compare our extensive simulations of the chemical Langevin equations with simulations of the master equation. We aim at a thorough characterization of the effect of intrinsic noise in the system of two coupled Brusselators by looking at the equal-time covariance and the corresponding correlation coefficient [see Eqs. (15) and (16)] for various dynamical regimes of the Brusselator model.

In Section 2, we discuss the effect of coupling two arbitrary chemical systems diffusively, and introduce our methodology of study. In Section 3, we study the equal-time cross-correlation of two coupled Brusselators taking separately into account deterministic coupling and intrinsic common noise. We conclude in Section 4 with a summary and discussion of our results.

2. Methodology and coupling mechanism

A chemical process at the microscopic level can be specified by a set of elementary processes which are symbolically written as a set of "reaction" channels

$$X_i + X_j + \cdots \xrightarrow{c_m} X_k + X_\ell + \cdots, \tag{2}$$

where the X represent the number of molecules of different chemical species (represented by the subscript), and c_m is the rate for the mth such channel. The time evolution of such a system can be treated as a stochastic process where the chemical species $X_i(t)$ are random variables. Such molecular fluctuations are often referred to as internal noise since their origin is in the very mechanism of the evolution of the state of the system [9]. The strength of the noise depends on the volume of the system and the reaction propensities and is not always small enough to be treated perturbatively.

As is well known, such a system is described by a master equation (ME) [9] for the evolution of configurational probabilities [9], which is written as

$$\frac{d}{dt}P(C,t) = \sum_{C'} P(C',t)W_{C'\to C} - \sum_{C'} P(C,t)W_{C\to C'}, \tag{3}$$

where $P(C,t)$ is the probability of configuration C at time t and $\{W\}$ are the transition probabilities.

One way to study such a system is by using stochastic simulation techniques [8]. The Gillespie algorithm [8] is consistent with the master equation formalism and gives a numerical method to study the time evolution of different chemical species. Alternatively, one can obtain the chemical Langevin equation (CLE) for the system, which provides an approximate description for sufficiently large system size [10]. In general, these will have the form

$$\frac{dX_i(t)}{dt} = \sum_{j=1}^{M} \nu_{ji} a_j(\mathbf{X}(t)) + \sum_{j=1}^{M} \nu_{ji} a_j^{1/2}(\mathbf{X}(t))\xi_j(t), \tag{4}$$

where ν_{ji} is the change in X_i produced by the jth reaction (typically, an integer number), $a_j(\mathbf{X}(t))$ is the propensity of jth reaction and $\xi_j(t)$ are temporally uncorrelated, statistically independent Gaussian white noises with $\langle \xi_i(t)\rangle = 0$ and $\langle \xi_i(t)\xi_j(t')\rangle = \delta_{ij}\delta(t-t')$. Note that the X_i's are treated as continuous rather than discrete variables and that the equations have to be interpreted in the sense of Ito [9]. This equation can be solved numerically by the simple Euler scheme:

$$X_i(t+dt) = X_i(t) + \sum_{j=1}^{M} \nu_{ji} a_j(\mathbf{X}(t))dt + \sum_{j=1}^{M} \nu_{ji} a_j^{1/2}(\mathbf{X}(t))N_j(t)(dt)^{1/2}, \tag{5}$$

where $N_j(t)$ are normally distributed variables with zero mean and unit variance. Instead of considering the number of molecules, we use in the following the concentrations $x_i = X_i/V$ (V is the volume) and their corresponding Langevin equations. Because the propensities a_i scale with the volume, the deterministic parts of the Langevin equations for the concentrations will be (largely) independent of the volume, whereas the stochastic force scales like $V^{-1/2}$.

Let us consider two uncoupled chemical systems with species denoted by X and X' and corresponding concentrations x and x', with identical reaction schemes and the same chemical rates. The Langevin equations for the two uncoupled systems will have the general form:

$$\dot{x} = f(x) + g(x,V)\xi_x(t), \tag{6}$$

$$\dot{x}' = f(x') + g(x',V)\xi_{x'}(t), \tag{7}$$

where $\xi_x(t)$ and $\xi_{x'}(t)$ are uncorrelated Gaussian white noises. The functional form of f and g depends on the actual reaction schemes and is given by Eq. (4). If we now couple the two systems diffusively via Eq. (1), following the prescription of Eq. (4), we obtain an additional deterministic interaction term in the drift term of the Langevin equation and an additional common noise term in the fluctuating driving force:

$$\dot{x} = f(x) + \varepsilon(x'-x) + g(x,V)\xi_x(t) - \sqrt{\frac{\varepsilon x}{V}}\xi_C^{(1)}(t) + \sqrt{\frac{\varepsilon x'}{V}}\xi_C^{(2)}(t), \tag{8}$$

$$\dot{x}' = f(x') + \varepsilon(x-x') + g(x',V)\xi_{x'}(t) + \sqrt{\frac{\varepsilon x}{V}}\xi_C^{(1)}(t) - \sqrt{\frac{\varepsilon x'}{V}}\xi_C^{(2)}(t). \tag{9}$$

Since $\xi_C^{(1)}(t)$ and $\xi_C^{(2)}(t)$ are independent noise sources $\left(\text{with } \left\langle \xi_C^{(i)}(t)\xi_C^{(j)}(t')\right\rangle = \delta_{(i)(j)}\delta(t-t')\right)$ appearing due to the coupling, we can write,

$$\sqrt{\frac{\varepsilon x}{V}}\xi_C^{(1)}(t) - \sqrt{\frac{\varepsilon x'}{V}}\xi_C^{(2)}(t) = \sqrt{\frac{\varepsilon(x+x')}{V}}\xi_C(t). \tag{10}$$

where $\xi_C(t)$ is an uncorrelated Gaussian white noise. Eqs. (8) and (9) is then written as,

$$\dot{x} = f(x) + \varepsilon(x'-x) + g(x,V)\xi_x(t) - \sqrt{\frac{\varepsilon(x+x')}{V}}\xi_C(t), \tag{11}$$

$$\dot{x}' = f(x') + \varepsilon(x-x') + g(x',V)\xi_{x'}(t) + \sqrt{\frac{\varepsilon(x+x')}{V}}\xi_C(t). \tag{12}$$

The deterministic interaction term has the usual form of Hookian spring and will be also referred in the following as the deterministic coupling. This term will typically lead to positive correlations between x and x'. The common noise term (the last one in both equations) is special in several respects. First, it enters both equations with opposite signs, i.e., the common noise terms affecting x and x' are actually anti-correlated. So, it is plausible that this term may lead to negative correlations or at least reduce positive correlations (which are due to the deterministic coupling). Secondly, the amplitude of the common noise is determined by the sum of x and x'. A sudden increase in either of the variables will lead to a sudden increase of the noise level in both systems. Below we will see an example where such an increase can also lead to positive correlations.

In order to contrast the effects of the deterministic coupling and the common noise, we label the different coupling contributions as ε_D and ε_C and rewrite Eqs. (11) and (12) as follows:

$$\dot{x} = f(x) + \varepsilon_D(x' - x) + g(x,V)\xi_x(t) - \sqrt{\frac{\varepsilon_C(x+x')}{V}}\xi_C(t), \tag{13}$$

$$\dot{x}' = f(x') + \varepsilon_D(x - x') + g(x',V)\xi_{x'}(t) + \sqrt{\frac{\varepsilon_C(x+x')}{V}}\xi_C(t). \tag{14}$$

With this labeling we can now compare the contributions of common noise coupling and deterministic coupling separately and hence can study the effect on the total correlation. We study the correlation properties for a general homogeneously coupled system for three different cases, namely (i) with both deterministic interaction and common noise present ($\varepsilon_D = \varepsilon_C \neq 0$), (ii) with only deterministic interaction present, the common noise artificially switched off ($\varepsilon_D \neq 0,\ \varepsilon_C = 0$), and (iii) with only common noise, the deterministic interaction being artificially switched off ($\varepsilon_D = 0,\ \varepsilon_C \neq 0$).

The correlation properties of the coupled system are studied by computing the equal-time cross-correlation function, namely the covariance $C_{xx'}$

$$C_{xx'} = \lim_{t\to\infty}[\langle x(t)x'(t)\rangle - \langle x(t)\rangle\langle x'(t)\rangle]. \tag{15}$$

The fraction of shared fluctuations between the systems is quantified by the cross-correlation coefficient $\rho_{xx'}$:

$$\rho_{xx'} = \lim_{t\to\infty}\frac{\langle x(t)x'(t)\rangle - \langle x(t)\rangle\langle x'(t)\rangle}{\sigma_x\sigma_{x'}} \equiv \frac{C_{xx'}}{\sigma_x\sigma_{x'}}, \tag{16}$$

where σ_x and $\sigma_{x'}$ are the standard deviations for the signals $x(t)$ and $x'(t)$, respectively. If $\rho_{xx'}$ is close to one, the two systems can be considered to be strongly coupled.

3. The Brusselator model

We study a model chemical reaction system, the so-called Brusselator, which has been extensively investigated before [28]. The Brusselator corresponds to the following reactions scheme [8]:

$$A_1 \xrightarrow{k_1} X, \tag{17}$$

$$A_2 + X \xrightarrow{k_2} Y + A_3, \tag{18}$$

$$2X + Y \xrightarrow{k_3} 3X, \tag{19}$$

$$X \xrightarrow{k_4} A_4. \tag{20}$$

Following Eq. (4), and writing in terms of concentrations x and y, the chemical Langevin equations corresponding to the reaction scheme of Eq. (17) is given by

$$\dot{x} = c_1 - c_2x + \frac{c_3}{2}x\left(x - \frac{1}{V}\right)y - c_4x + \varepsilon(x' - x) + \sqrt{\frac{c_1}{V}}\xi_1(t) - \sqrt{\frac{c_2x}{V}}\xi_2(t) + \sqrt{\frac{c_3}{2V}x\left(x - \frac{1}{V}\right)y}\xi_3(t) - \sqrt{\frac{c_4x}{V}}\xi_4(t), \tag{21}$$

$$\dot{y} = c_2x - \frac{c_3}{2}x\left(x - \frac{1}{V}\right)y + \sqrt{\frac{c_2x}{V}}\xi_2(t) - \sqrt{\frac{c_3}{2V}x\left(x - \frac{1}{V}\right)y}\xi_3(t), \tag{22}$$

where $x = X/V$ and $y = Y/V$. The new parameters c_i's are given by $c_1 = k_1\frac{A_1}{V}$, $c_2 = k_2\frac{A_2}{V}$, $c_3 = k_3$ and $c_4 = k_4$, respectively ($A_1(V)/V$ and $A_2(V)/V$ are the volume-independent concentrations of the reservoir molecules).

In the macroscopic limit ($V \to \infty$), one can derive a set of deterministic reaction-rate equations for the average concentrations,

$$\dot{x} = c_1 - c_2x + \frac{c_3}{2}x^2y - c_4x, \tag{23}$$

$$\dot{y} = c_2x - \frac{c_3}{2}x^2y. \tag{24}$$

By suitably varying the parameters in Eqs. (23) and (24), one gets either limit cycle or stationary solutions.

One can write the condition for Hopf bifurcation from the trace condition (see Appendix A) in terms of two parameters a and b, as

$$(2a-1)(1-a)^2 = b, \tag{25}$$

where $a = c_2/(c_2 + c_4)$ and $b = (c_1^2c_3)/[2(c_2 + c_4)^3]$. In Fig. 1, we plot Eq. (25) in $(a - b)$ parameter space, which divides the regions of limit cycle (dark) and fixed point (grey) behavior. In the present work we obtain a, b values by varying c_1 and c_4, whereas c_2 and c_3 are kept fixed (see Table 1).

The nature of the oscillations depends on the position inside the dark region in Fig. 1. For example, in Fig. 2, we compare two different oscillatory behaviors corresponding to the parameter sets II and IV (see Table 1). Point II corresponds to a smooth limit-cycle behavior with comparable time-scales, whereas for point IV relaxation oscillations due to alternating slow and fast dynamics are observed. We also inspect the statistics at two points close to the Hopf bifurcation line but situated in the stable-fixed-point regime. Point III is chosen close to the left boundary where the transition to the limit-cycle behavior is smooth, i.e., the amplitude of the limit cycle grows slowly on crossing the Hopf bifurcation. At point V, in contrast, the behavior of the system is excitable, implying that

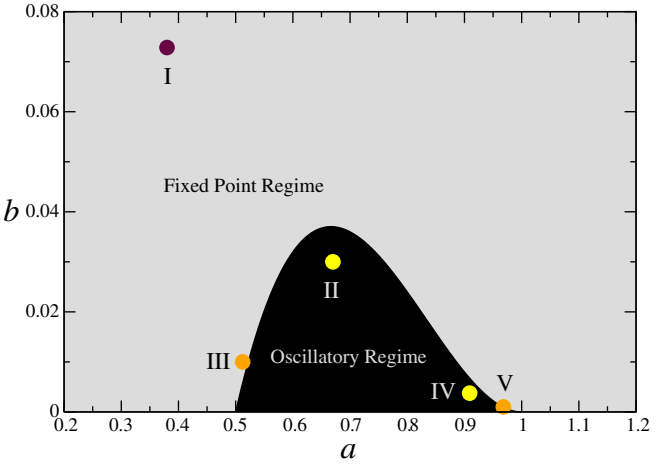

Fig. 1. Dynamical behavior in the $(a - b)$ parameter space. The grey and the dark regions corresponds to fixed point behavior and oscillatory behaviors, respectively. The boundary between the two shows the Hopf bifurcation transition from one dynamical behavior to the other. We study the correlation properties in the labeled points (I–V). Point II is compared with point IV in Fig. 2. All the parameter values are given in Table 1. (For interpretation of the references in color in this figure legend, the reader is referred to the web version of this article.)

Table 1
Parameter values for points (I–V) of the chemical Brusselator in Fig. 1; in all cases $c_2 = 50,\ c_3 = 5 \times 10^{-5}$.

Re	a	b	c_1	c_4
I	0.384	7.28×10^{-2}	8.0×10^4	80
II	0.667	3.0×10^{-2}	2.25×10^4	25
III	0.5123	9.9955×10^{-3}	1.9279×10^4	47.599
IV	0.9091	3.75×10^{-3}	5.0×10^3	5
V	0.968	1.0×10^{-3}	2.348×10^3	1.653

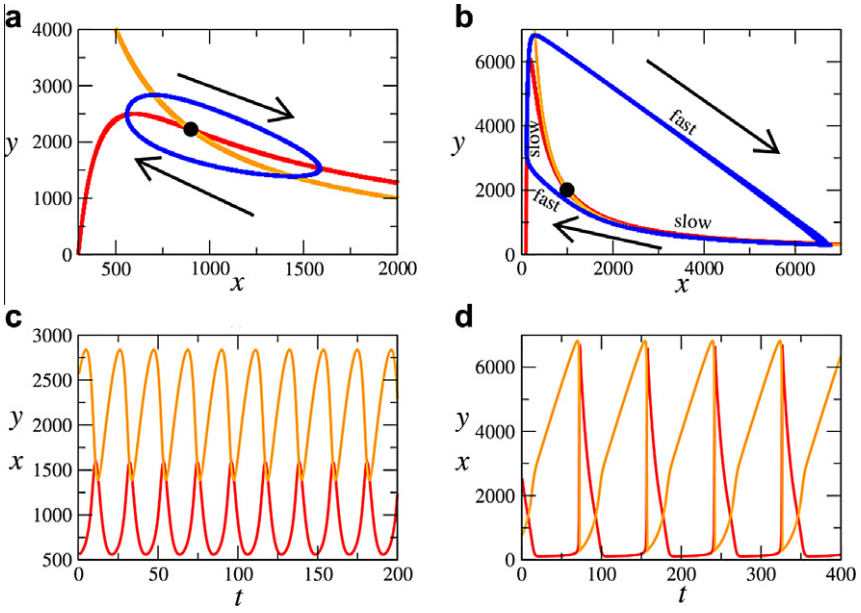

Fig. 2. Comparison of different limit-cycle behaviors for a single Brusselator model for different parameters. (a) Phase portrait (blue) plotted along with the null-clines of x (red) and the y (orange) for point II (arrows indicate direction of motion along the limit cycle). The time-scales of x and y are comparable giving rise to a smooth limit cycle as seen in (c) where the corresponding time series of x and y variables are plotted. (b) Phase portrait and null-clines for the relaxation oscillator (point IV). The different regimes of slow and fast dynamics along the limit cycle are specified. The corresponding time-series are shown in (d). (For interpretation of the references in color in this figure legend, the reader is referred to the web version of this article.)

a sufficiently strong perturbation elicits a large stereotypical response corresponding to one detour in phase space [29].

In the following, we consider two Brusselators coupled diffusively through species X and X'. The system is then enlarged to

$$\begin{aligned}
&A_1 \xrightarrow{c_1} X, \quad A_1 \xrightarrow{c_1'} X',\\
&A_2 + X \xrightarrow{c_2} Y + A_3, \quad A_2 + X' \xrightarrow{c_2'} Y' + A_3,\\
&2X + Y \xrightarrow{c_3} 3X, \quad 2X' + Y' \xrightarrow{c_3'} 3X',\\
&X \xrightarrow{c_4} A_4, \quad X' \xrightarrow{c_4'} A_4,\\
&X \underset{\varepsilon}{\overset{\varepsilon}{\rightleftharpoons}} X'.
\end{aligned} \tag{26}$$

Previous studies have focused on phase synchronization of the two Brusselators in the inhomogeneous system (i.e., $c_i \neq c_i'$) [27] and on the effect of coupling via the variable Y [30]. In this work we consider the homogenous case, i.e., $c_i = c_i'$. Similarly as before, the CLE corresponding to the reaction scheme of Eq. (26) can be written as follows:

$$\begin{aligned}
\dot{x} &= f_x(x,y) + \varepsilon_D(x' - x) + \frac{g_x(x)}{\sqrt{V}}\xi_x(t) + \frac{g_y(x,y)}{\sqrt{V}}\xi_y(t) - \sqrt{\frac{\varepsilon_C(x+x')}{V}}\xi_C(t),\\
\dot{y} &= f_y(x,y) - \frac{g_y(x,y)}{\sqrt{V}}\xi_y(t),\\
\dot{x}' &= f_x(x',y') + \varepsilon_D(x - x') + \frac{g_x(x')}{\sqrt{V}}\xi_{x'}(t) + \frac{g_y(x',y')}{\sqrt{V}}\xi_{y'}(t)\\
&\quad + \sqrt{\frac{\varepsilon_C(x+x')}{V}}\xi_C(t),\\
\dot{y}' &= f_y(x',y') - \frac{g_y(x',y')}{\sqrt{V}}\xi_{y'}(t),
\end{aligned} \tag{27}$$

where $f_x(x,y) = c_1 - c_2x + c_3x(x-1/V)y/2 - c_4x$, $f_y(x,y) = c_2x - c_3x(x-1/V)y/2$, $g_x(x) = \sqrt{c_1 + c_4\bar{x}}$, $g_y(x,y) = \sqrt{[c_2 + c_3(x-1/V)y/2]\bar{x}}$ and noise terms with different indices are statistically independent.

The CLE remains an approximation to the master equation that is valid only for sufficiently large system size (volume V). In particular, the CLE fails if particle numbers are small and thus the discrete character of the stochastic problem becomes apparent. A criterion for the validity of the approximation is thus whether particle numbers are likely to be small, i.e., whether the steady-state probability for a certain species to be below a certain threshold is sufficiently small. Following this idea, we define a critical system size V_{cr}, below which the Langevin description is not reliable, in the following way. At a fixed volume, we obtain by simulation of the master equation a long trajectory of the number of molecules of the species X. From this we estimate the probability of the variable to be below a certain threshold value (here we choose $X_{threshold} = 2$), i.e., $P(X < X_{threshold})$. By repeating this estimation for different volumes, we find the volume for which $P(X < X_{threshold}) \approx 0.1$, i.e., the probability to find a particle number below 2 is 10%. This volume is defined as the critical one and indicated by vertical dashed lines in Figs. 4, 6, 7, and 9.

In the next section, we study the correlation properties for the above system in the different dynamical regimes (see Fig. 1), namely stationary (I), oscillatory (II and IV) and close to the bifurcation line (III and V). The master equation is simulated with a simple Monte-Carlo algorithm while we use a simple Euler procedure according to Eq. (5) for the different versions of the chemical Langevin equation. For the Langevin equation, we perform simulations with only the deterministic coupling, only with common noise, or with both coupling-induced terms.

3.1. Fixed-point behavior (point I)

This parameter set (point I in Fig. 1) corresponds to a stable fixed point far away from the bifurcation boundary. We first explain the correlation statistics for varying system size and coupling strength (Fig. 3) as seen in the simulation of the master equation (orange lines).

For small system size, the concentrations of the species x and x' fluctuate about a steady-state value which corresponds to the stable fixed point. The amplitude of the fluctuations decays as we go to larger system size (not shown). This also reduces the covariance $C_{xx'}$ between the two systems (Fig. 3a). However, the ratio between

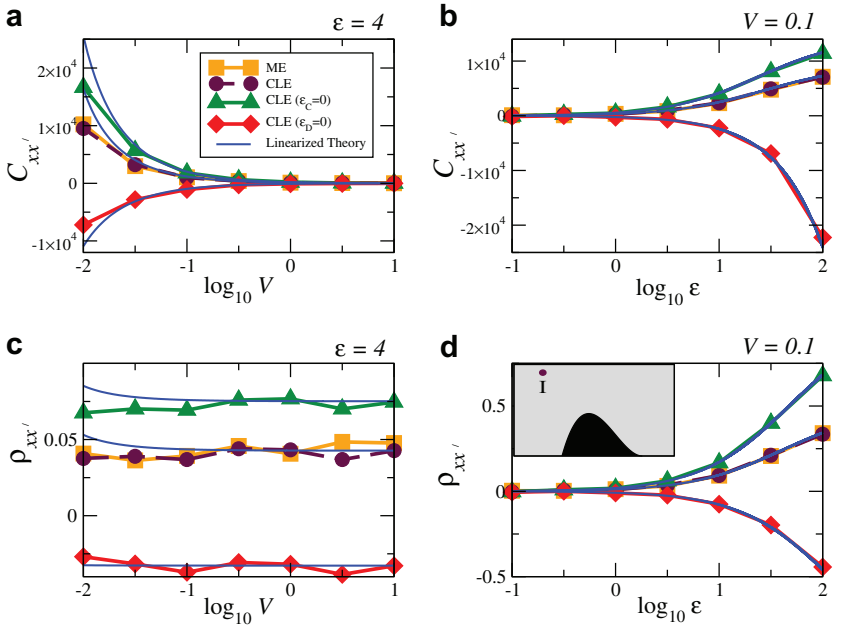

Fig. 3. Correlation between x and x' for the stationary case (point I in Fig. 1) for (i) $\varepsilon_D = \varepsilon_C \neq 0$ (maroon), (ii) $\varepsilon_D \neq 0,\ \varepsilon_C = 0$ (green), and (iii) $\varepsilon_D = 0,\ \varepsilon_C \neq 0$ (red), obtained by CLE simulation. These are compared with the ME simulations (orange). (a) $C_{xx'}$ versus system size at fixed coupling ($\varepsilon = 4$). (b) $C_{xx'}$ as a function of coupling strength (for the three Langevin equation cases: $\varepsilon = \varepsilon_D = \varepsilon_C$ (i), $\varepsilon = \varepsilon_D,\ \varepsilon_C = 0$ (ii), and $\varepsilon = \varepsilon_C,\ \varepsilon_D = 0$ (iii)) at a fixed system size ($V = 0.1$). Similar plots are obtained for $\rho_{xx'}$ in (c) and (d), respectively. For all the cases we compare the results with the linearized theory (blue lines). (For interpretation of the references in color in this figure legend, the reader is referred to the web version of this article.)

covariance and variance, i.e., the correlation coefficient $\rho_{xx'}$, remains approximately constant (Fig. 3c). Because the two Brusselators show only small fluctuations around their respective fixed point, their behavior is similar to that of two coupled linear systems for which the correlation coefficient indeed does not depend on the system size. Fixing the volume to a small value and varying the coupling, we observe an increase in both the covariance and the correlation coefficient (Fig. 3b and d).

Turning to the Langevin simulation with both deterministic coupling and common noise (maroon lines), we first note the excellent agreement with the results from the master equation. The critical volume is rather small in the stable-fixed point case and is outside the region of system sizes considered ($V_{cr} < 0.01$). As pointed out above, the fluctuations around the steady-state are rather small implying that the number of molecules falls rarely below $X_{threshold}$.

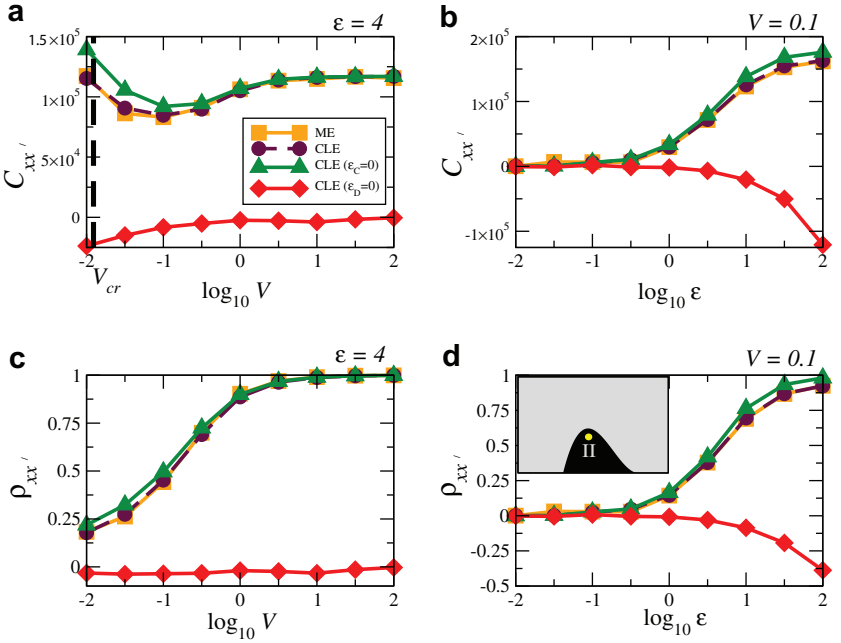

Fig. 4. Correlation between x and x' (similar to Fig. 3) in oscillatory regime (point II in Fig. 1). (a) $C_{xx'}$ versus system size at a fixed coupling strength ($\varepsilon = 4$). The dashed line labels the critical volume ($V_{cr} \sim 0.013$). (b) $C_{xx'}$ versus coupling strength (for the three Langevin equation cases: $\varepsilon = \varepsilon_D = \varepsilon_C$ (i), $\varepsilon = \varepsilon_D,\ \varepsilon_C = 0$ (ii), and $\varepsilon = \varepsilon_C,\ \varepsilon_D = 0$ (iii)) at a fixed volume ($V = 0.1$). Similarly $\rho_{xx'}$ versus system size and coupling in (c) and (d), respectively. (For interpretation of the references in color in this figure legend, the reader is referred to the web version of this article.)

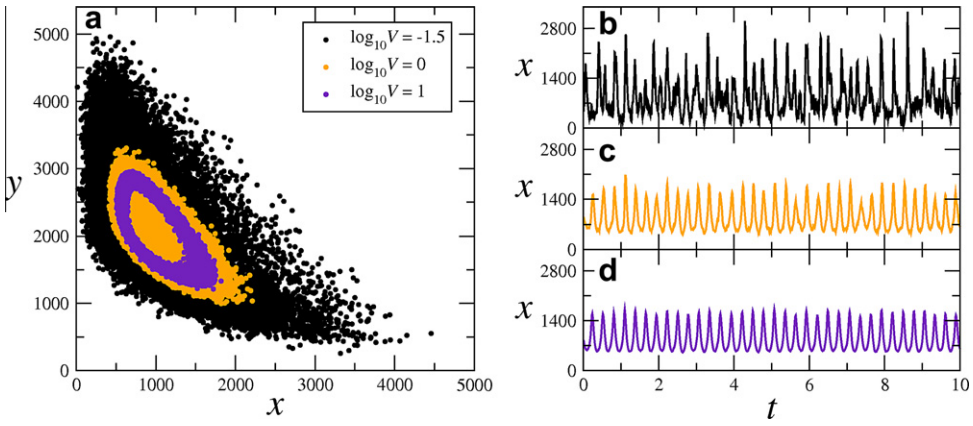

Fig. 5. Behavior of the smooth oscillator dynamics (parameter set II) at different system sizes. (a) Phase-portrait at three different volumes (see legend) illustrating the (clockwise) motion on the limit cycle with noise-dependent amplitude. At small volume (black points) corresponding to a large noise intensity, the diameter of the limit cycle is large and, consequently, $x(t)$ as demonstrated in (b) possesses a large variance. At moderate (orange) and large (indigo) volume, the limit cycle shrinks towards its deterministic size and, thus, the variability of $x(t)$ decreases to that given by the deterministic oscillation [cf. (c) and (d), and red line in Fig. 2c]. (For interpretation of the references in color in this figure legend, the reader is referred to the web version of this article.)

Switching off the common noise (green lines), the covariance (Fig. 3a and b) as well as the correlation coefficient (Fig. 3c and d) between the Brusselators increase. In particular, $\rho_{xx'}$ increases by a factor of two when no common noise is present (Fig. 3c). Because the common noise is anti-correlated in the dynamics of x and x', it counteracts the positive correlations and reduces them. Consequently, without the anti-correlated common noise, positive correlations become stronger. This picture is further supported by our simulations with only common noise but without deterministic coupling (red lines in Fig. 3). A clear negative correlation is observed in this case.

In Fig. 3, we also plot the covariance and the correlation coefficient from the linearized theory (blue lines) and compare with the simulations. The theoretical lines are in very good agreement with the simulation results except at small system sizes (Fig. 3a and c), where one observes a systematic deviation. This is due to the fact that we approximate the multiplicative noise terms as additive noise sources with an intensity evaluated at the stationary point. This approximation fails at very small system size where the effects of multiplicative noise become crucial. The details for solving the linearized Langevin equation and obtaining the cross-correlation coefficients are discussed in Appendix B.

3.2. Smooth oscillations (point II)

For this parameter set (point II in Fig. 1), x and x' oscillate with relatively small amplitudes (see Fig. 2a and c for an example of the deterministic case $V \to \infty$). As before we first focus on the correla-

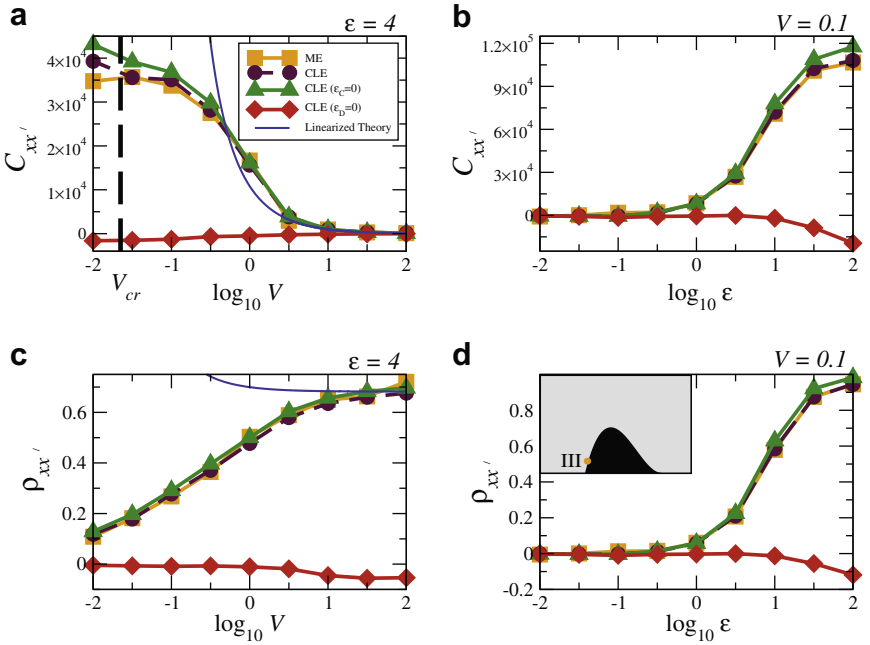

Fig. 6. Correlation between x and x' close to the bifurcation at the left boundary (point III in Fig. 1). (a) $C_{xx'}$ versus system size at fixed coupling ($\varepsilon = 4$). The dashed line labels the critical volume ($V_{cr} \sim 0.022$). (b) $C_{xx'}$ versus coupling strength (for the three Langevin equation cases: $\varepsilon = \varepsilon_D = \varepsilon_C$ (i), $\varepsilon = \varepsilon_D$, $\varepsilon_C = 0$ (ii), and $\varepsilon = \varepsilon_C$, $\varepsilon_D = 0$ (iii)) at a fixed volume ($V = 0.1$). Similar plots are obtained for $\rho_{xx'}$ versus system size and coupling in (c) and (d), respectively. In (a) and (c), we also compare the results for the full CLE (maroon lines) with the linearized theory for this case (blue line). (For interpretation of the references in color in this figure legend, the reader is referred to the web version of this article.)

tions statistics for the master equation simulations (orange lines in Fig. 4).

The covariance (Fig. 4a) first decreases with increasing volume, reaches a minimum, and then increases again to saturate in the deterministic limit. In order to understand the decrease at small volume, we show in Fig. 5 the stochastic limit cycles in the Langevin approximation for three different volumes. By increasing an initial small volume of $\log_{10}V = -1.5$ to $\log_{10}V = 0$ and further to $\log_{10}V = 1$ the amplitude of the limit cycle for both Brusselators shrinks considerably and will be further reduced upon increasing the volume to the small deterministic limit cycle shown in Fig. 2a. Put differently, the intrinsic noise of the finite system translates not only into a phase noise for the motion along the limit cycle but also into strong amplitude fluctuations. The decrease in the variance with growing system size is the reason for the initial decrease in the covariance. This is also supported by the observation that the correlation coefficient, i.e., the amplitude-normalized correlation, *increases* with growing volume (Fig. 4c). The plateau at large system size indicates complete synchronization of the two oscillators – all the variance and covariance in this deterministic limit is due to the motion along the limit cycle which is seen as an oscillation in $x(t)$. Note that complete synchronization is achieved at arbitrarily small coupling strength, because we consider two identical oscillators. Synchronization of the systems can be also observed at small system size if the coupling in sufficiently increased. As demonstrated in Fig. 4b and d both the covariance and the correlation coefficient are monotonically increasing functions of the coupling strength that saturate at about $\varepsilon = 100$.

The Langevin simulation including both deterministic coupling and common noise (maroon lines in Fig. 4) is again in excellent agreement with the master equation simulation as long as the system size is larger than the critical volume (here $V_{crit} \simeq 0.013$). Without common noise (green lines), the correlation becomes larger – an effect that is particularly well seen at small system size where the noise (and not the limit-cycle motion) makes the strongest contribution to the covariance. Thus, neglecting the common noise can lead to an overestimation of the correlation and may result in an error of about 20%.

Common noise alone (red lines) leads as in the stable-fixed point case to negative correlations because the common noise terms enter with different signs in the dynamics of x and x'. Clearly, the deterministic coupling is the dominating factor in the correlation statistics.

3.3. Close to the bifurcation at the left boundary (point III)

In this case we are in the fixed-point regime but very close to the bifurcation boundary on the left side (point III in Fig. 1). On crossing the boundary one observes small-amplitude oscillations as typical for a supercritical Hopf bifurcation.

The simulation of the master equation (orange lines in Fig. 6) reveal a covariance of x and x' that decreases with increasing system size (Fig. 6a). Similarly to the oscillatory case considered in the previous subsection, this is caused by a reduction of the overall amplitudes of the two Brusselators. The correlation coefficient, in contrast, increases monotonically with V and saturates at a value about 0.6 (see Fig. 6c). Thus, in marked contrast to the case of a fixed point far away from the bifurcation, here $\rho_{xx'}$ depends strongly on the volume (cf. Fig. 6c to Fig. 3c). This is due to the nonlinearity of the dynamics that becomes noticeable at sufficiently high intrinsic noise (i.e., sufficiently small volume).

Again we find the same agreement between simulations of the master equation (orange lines) and of the full Langevin equations including both deterministic coupling and common noise (maroon lines). Interestingly, when we switch off the common noise (green lines), the correlations increase slightly as in the cases considered above but remain close to the full Langevin and the master equation simulations; deviations from the full solution are largest at small volume (cf. Fig. 6a) and large coupling (cf. Fig. 6b and d). With only common noise but without deterministic coupling (red lines), we observe again a slight negative correlation between x and x' for the same reason as in the previous cases, i.e., because

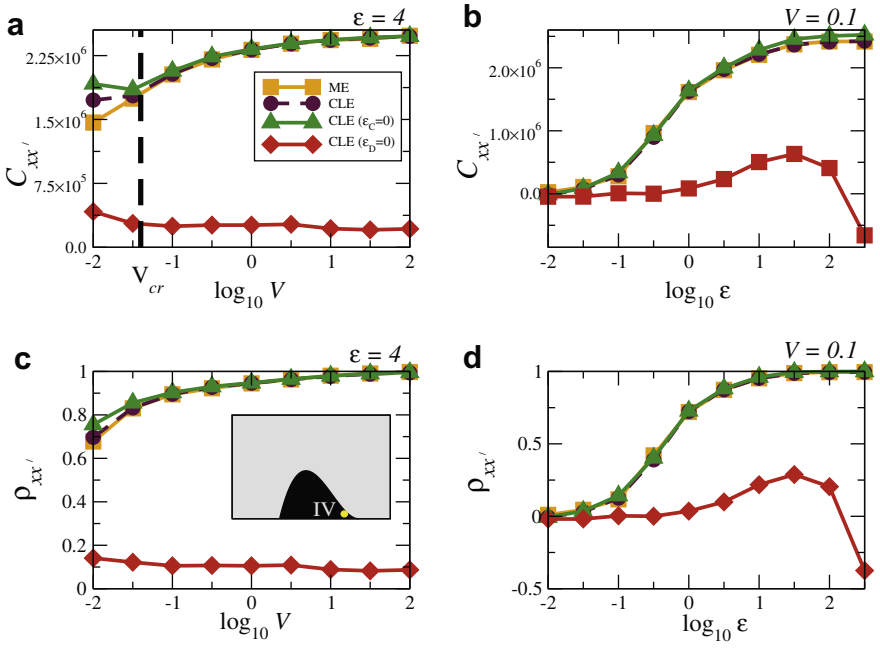

Fig. 7. Correlation between x and x' in oscillatory regime (point IV in Fig. 1). (a) $C_{xx'}$ versus system size at a fixed coupling strength ($\varepsilon = 4$). The dashed line labels the critical volume ($V_{cr} \sim 0.04$). (b) $C_{xx'}$ versus coupling strength (for the three Langevin equation cases: $\varepsilon = \varepsilon_D = \varepsilon_C$ (i), $\varepsilon = \varepsilon_D$, $\varepsilon_C = 0$ (ii), and $\varepsilon = \varepsilon_C$, $\varepsilon_D = 0$ (iii)) at a fixed volume ($V = 0.1$). Similarly $\rho_{xx'}$ versus system size and coupling in (c) and (d), respectively. (For interpretation of the references in color in this figure legend, the reader is referred to the web version of this article.)

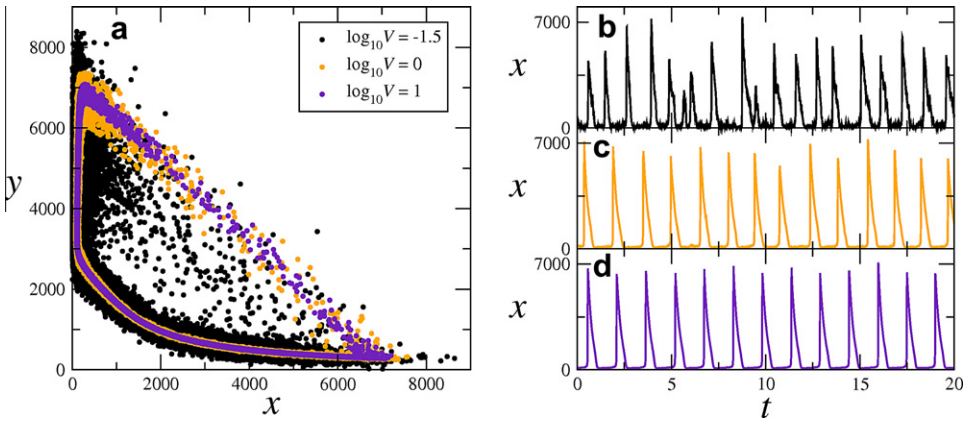

Fig. 8. Behavior of the relaxation oscillator dynamics (parameter set IV) at different system size. (a) Phase-portrait at three different volumes (see legend) illustrating the motion on the limit cycle (clock-wise motion). At small volume (black points) corresponding to a large noise intensity, the trajectory takes "short-cuts" which make the pulse height in $x(t)$ variable and reduce their mean value as demonstrated in (b). At moderate (orange) and large (indigo) volume, the pulse height becomes larger and less variable [cf. (c) and (d)], resulting in a larger variance of $x(t)$. (For interpretation of the references in color in this figure legend, the reader is referred to the web version of this article.)

of the anti-correlation of the common-noise terms in the dynamics of x and x'.

We also plot the covariance and the correlation coefficient from the linearized theory (blue lines) and compare with the simulations. The theoretical lines agree with the simulation results only on approaching large system size (Fig. 3a and c). This is due to the fact that close to the bifurcation nonlinearities become crucial already at intermediate system size.

3.4. Relaxation oscillations (point IV)

In this case we observe relaxation oscillations (point IV in Fig. 1) where x and x' oscillate with much larger amplitudes and alternate between regions of fast and slow motion along their limit cycles (see Fig. 2b and d for a comparison).

In Fig. 7a, the master equation simulation (orange lines) reveals that the covariance of x and x' increases monotonically with increasing system size until it saturates to a fixed value as one approaches the deterministic limit. This is in contrast to the smooth oscillatory case in Fig. 4a where we observed a minimum of the covariance versus volume. In this latter case, the smooth limit cycle (parameter set II) is significantly enlarged by noise [cf. Fig. 5], whereas the amplitude of the relaxation oscillator considered here decreases slightly with increasing levels of noise. The latter effect is illustrated in Fig. 8: noise allows the trajectory to take short-cuts along the limit cycle (corresponding to the upstroke in $x(t)$) which leads on average to smaller pulses and thus to a reduced variance. So increasing the volume results in larger pulses in $x(t)$ and will thus also increase the covariance. At the same time, a reduced intrinsic noise allows the two oscillators to synchronize their mo-

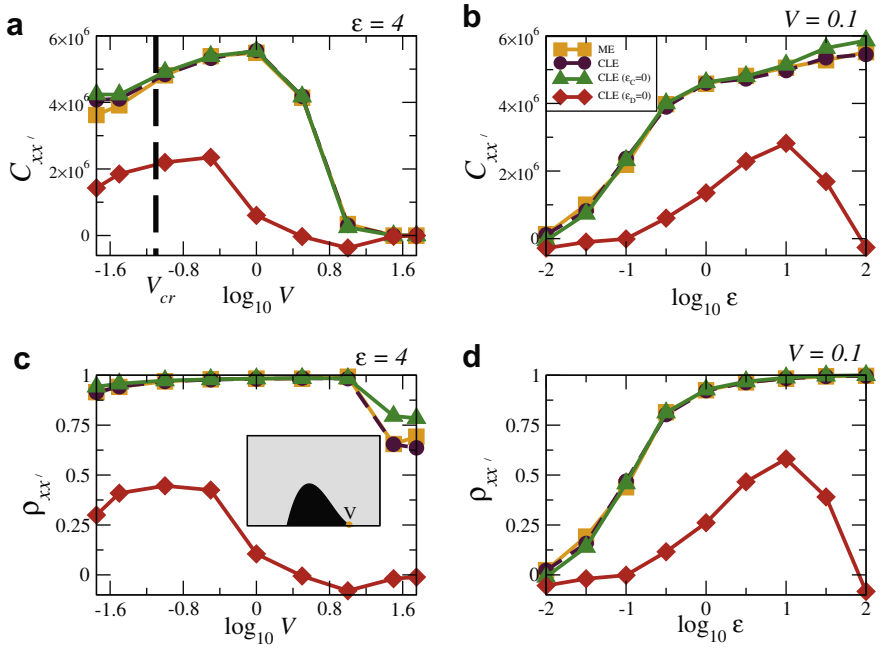

Fig. 9. Correlation between x and x' for the excitable case (point V in Fig. 1). (a) $C_{xx'}$ versus system size at fixed coupling ($\varepsilon = 4$). The dashed line labels the critical volume ($V_{cr} \sim 0.08$). (b) $C_{xx'}$ versus coupling strength (for the three Langevin equation cases: $\varepsilon = \varepsilon_D = \varepsilon_C$ (i), $\varepsilon = \varepsilon_D$, $\varepsilon_C = 0$ (ii), and $\varepsilon = \varepsilon_C$, $\varepsilon_D = 0$ (iii)) at a fixed volume ($V = 0.1$). Similar plots for $\rho_{xx'}$ versus system size and coupling in (c) and (d), respectively. (For interpretation of the references in color in this figure legend, the reader is referred to the web version of this article.)

tions around the limit cycle better. Both effects contribute to the growth of covariance with increasing volume. Because of the enhanced synchronization at large volume, the correlation coefficient also increases monotonically with increasing system size [cf. Fig. 7c]. In Fig. 7b and d, we demonstrate that the covariance and the correlation coefficient show a likewise monotonic increase with the coupling strength; saturation occurs at $\varepsilon \approx 10$.

The Langevin simulation including both deterministic coupling and common noise (maroon lines) is again in very good agreement with the master equation simulations as long as the system size is above the critical volume (here $V_{crit} \simeq 0.04$). The critical volume is larger than in the previous cases due to the fact that the concentrations x and x' attain very low values during their stochastic oscillation cycles.

In the case of relaxation oscillations, the common noise does not have a significant impact (see Fig. 7). Neglecting the common noise terms (green lines), the correlations are close to the one obtained from full Langevin simulations (maroon lines) and the results of the Master equation (orange lines). Curiously, if we only use the common noise term but neglect the deterministic coupling, we observe also a *positive* correlation between the oscillators in marked contrast to the negative correlations that were seen in this scenario for the parameter sets I–III. We have found that this positive correlation is due to a noise-induced synchronization between the oscillators. We recall that the intensity of the common noise term depends on the values x and x'. If one oscillator attains large values of x (or x'), this increases strongly the common noise term in both oscillators. In many systems an increased noise increases the instantaneous speed of a noisy limit-cycle oscillator (see e.g. [31] and the inset of Fig. 4 therein). Under circumstances that are met for parameter set IV (and also V, see below), the noise-induced speedup can partially synchronize the oscillators. Interestingly, this synchronization effect is maximized at a finite strength of the coupling-induced common noise [cf. Fig. 7d, red line].

3.5. Excitable behavior (point V)

In this case we are in the fixed point regime but close to the bifurcation boundary on the right side (point V in Fig. 1). On crossing the boundary, one would observe relaxation oscillations.

The master equation simulation in Fig. 9a [orange lines] shows that the covariance between x and x' increases initially with increasing system size, reaches a maximum value and then decreases towards zero at larger volume. In other words, there is an optimal volume (noise level) that maximizes the correlation between the Brusselators. A maximum is also found for the correlation coefficient as a function of system size, although at higher volume [cf. Fig. 9c]. Both maxima rely on the fact that the system at point V is excitable. Whereas the covariance and correlation coefficient increase at small volume for the very same reasons as discussed for the relaxation oscillator case, both functions drop at high volume because in the excitable regime the spiking stops when the intensity of the intrinsic noise tends to zero. This is also true for the variance of the system as illustrated in Fig. 10.

Turning to the Langevin simulations with both deterministic coupling and common noise (maroon curves), we find excellent agreement with the master equation simulations. Switching off the common noise (green lines), the correlations always remain close to the full Langevin description and the master equation simulations, showing that the common noise plays a negligible role. For the Langevin simulations with only intrinsic common noise present (red lines), the covariance and the correlation coefficients are both positive and show also maxima versus system size.

4. Discussion

Coupling between chemical processes arises in various cellular and sub-cellular processes. Diffusion of molecules accounts for inter- or intra-cellular signaling. Coupling by diffusion has been recently studied in the biological context [16,5,4,17]. For instance, artificial gene regulatory networks have been suggested wherein individual networks are coupled across cells via diffusion of so-called auto-inducer molecules [16,5,4]. Although the master equation formalism is best for studying such intrinsically stochastic systems, for moderately large systems the corresponding Langevin description is sometimes more transparent and convenient for analysis.

In this work we have shown that coupling through diffusion of chemical species gives rise to an intrinsic common noise term in the Langevin picture. We extensively studied various dynamical regimes of the coupled Brusselator system by means of the master equation and the Langevin description. The latter allowed us to artificially switch off one of the coupling terms (either deterministic coupling or common noise) and thus to gauge their effect on the correlation of the two Brusselators. Our distinction between coupling-induced common noise and deterministic coupling makes

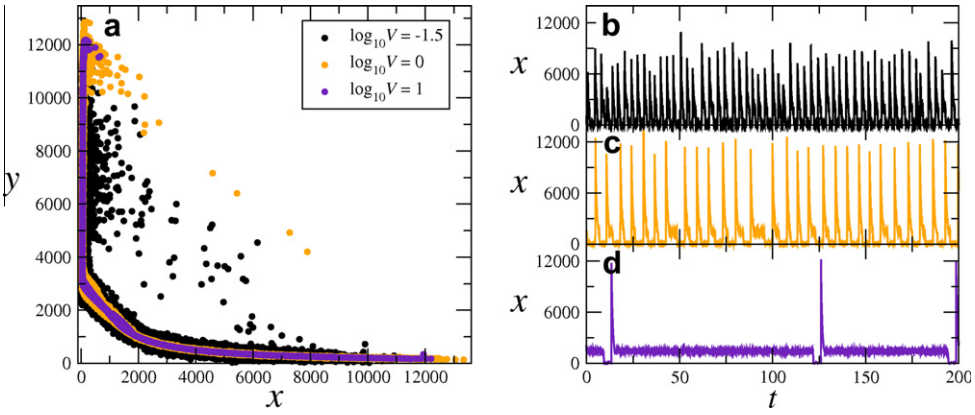

Fig. 10. Behavior of the excitable dynamics (parameter set V) at different system size. (a) Phase-portrait at three different volumes (see legend) illustrating the (clock-wise) motion around the noise-induced limit cycle. At small volume (black points) corresponding to a large noise intensity, the trajectory takes "short-cuts" which diminishes the height of the pulses in $x(t)$ shown in (b). At moderate volume (orange), the pulse rate is lowered but the pulse height is large and does not vary (c) – here $x(t)$ possesses maxima in variance and covariance versus volume [cf. Fig. 9a]. Upon further increasing the volume (indigo), spiking becomes rare because the excitable system resides most of the time around its stable fixed point, which leads to a small value of the variance for $x(t)$ [cf. (d)]. (For interpretation of the references in color in this figure legend, the reader is referred to the web version of this article.)

sense only at the level of the chemical Langevin equation and therefore requires the validity of this equation. We compared throughout our Langevin equation simulations with simulations of the original master equation which were found to be in very good agreement.

For all inspected parameter sets, results of Langevin simulations with only deterministic coupling are qualitatively similar to those of the Langevin simulations of the full system and to the master equation. In contrast, the Langevin simulations with only common noise showed in most cases a qualitatively different behavior (leading, for instance, to negative instead of positive correlations). In general, neglecting the common noise term results in a quantitative error compared to the master equation simulations; this error is largest at small volume and large coupling in all cases considered.

Regarding the influence of the operation point of the system on the significance of the intrinsic common noise, we observed the following. In the stable-fixed point regime, the common noise makes a significant contribution to the total correlation. This contribution decreases as we go from the linear stable-fixed point regime via the smooth-oscillatory regime to the relaxation-oscillator regime. Roughly speaking, the effect of the common noise decreases as the dynamics of the Brusselator "becomes more nonlinear". As a consequence, for parameter sets where the system displays relaxation oscillations or an excitable behavior, the common noise term can be safely neglected for all volumes and coupling strengths for which the Langevin description is valid.

Our work is a first step in understanding the effect of intrinsic common noise arising due to diffusive coupling. We considered here a minimal model of two chemical Brusselators coupled via diffusion of a single chemical species where the effect of the common noise was rather modest. One could also consider non-identical oscillators, diffusion of more than one species, and more than two coupled chemical systems. Such scenarios will give rise to multiple deterministic interaction and intrinsic common noise terms. It is not clear how the latter will affect the dynamics of the coupled system and whether in some situations common noise could dominate the correlations among the systems.

Besides the study of the importance of intrinsic common noise in the two coupled systems, we found two remarkable noise-induced effects on the correlation of the two Brusselators. The covariance can be *minimized* for a certain volume (i.e., for a finite level of intrinsic noise) if the single system exhibits smooth oscillations with an amplitude dynamics significantly affected by noise. Secondly, for the Brusselators operating in a strongly excitable regime the covariance and also the correlation coefficient between the oscillators can be *maximized* at a finite system size, i.e., at a finite level of the intrinsic noise. For a single Brusselator system [32] in the excitable regime as well as for other excitable systems with chemical noise [6,33], effects induced by varying the intrinsic noise (via changing the system size) have been explored. In particular, it has been shown [32] that the regularity of the pulse train in the excitable Brusselator is maximized at a finite level of intrinsic noise, an effect known as intrinsic coherence resonance [6]. How the maxima in correlation and in pulse train coherence are related is an interesting problem for future studies.

Appendix A. Stability analysis of the deterministic system

Here we outline the stability analysis (applying standard techniques, see e.g. [34]) in terms of the effective parameters a and b. It is convenient to reduce the number of parameters in the deterministic Brusselator model by scaling the time variable $\tilde{t} = (c_2 + c_4)t$ by which Eqs. (23) and (24) turns into

$$\dot{x} = \tilde{c}_1 - x + \tilde{c}_3 x^2 y, \tag{A.1}$$

$$\dot{y} = \tilde{c}_2 x - \tilde{c}_3 x^2 y, \tag{A.2}$$

where $\tilde{c}_1 = c_1/(c_2 + c_4)$, $\tilde{c}_2 = c_2/(c_2 + c_4)$ and $\tilde{c}_3 = c_3/2(c_2 + c_4)$, respectively.

In terms of the new constants the null-clines of the system of Eqs. (A.1) and (A.2) are given by

$$y^{\dot{x}=0} = \frac{x - \tilde{c}_1}{\tilde{c}_3 x^2}, \quad y^{\dot{y}=0} = \frac{\tilde{c}_2}{\tilde{c}_3 x} \tag{A.3}$$

leading to the fixed point $x_0 = \tilde{c}_1/(1 - \tilde{c}_2)$, $y_0 = \tilde{c}_2(1 - \tilde{c}_4)/\tilde{c}_1\tilde{c}_3$. The Jacobian at the stationary point is,

$$J = \begin{bmatrix} 2\tilde{c}_2 - 1 & \frac{\tilde{c}_1^2\tilde{c}_3}{(1-\tilde{c}_2)^2} \\ -\tilde{c}_2 & -\frac{\tilde{c}_1^2\tilde{c}_3}{(1-\tilde{c}_2)^2} \end{bmatrix}, \tag{A.4}$$

and its trace is given by

$$Tr = (2\tilde{c}_2 - 1) - \frac{\tilde{c}_1^2\tilde{c}_3}{(1-\tilde{c}_2)^2} = (2a - 1) - \frac{b}{(1-a)^2}, \tag{A.5}$$

where $a = \tilde{c}_2$ and $b = \tilde{c}_1^2\tilde{c}_3$. This leads to the condition for the Hopf bifurcation equation (25). For $Tr < 0$, the system possesses a stable fixed point, whereas for $Tr > 0$, the fixed point is unstable and the dynamics becomes oscillatory. Fig. 1 shows the points of limit-cycle and fixed-point behavior in the $(a - b)$ parameter space.

Appendix B. Correlation of the linearized system

For the case of a stable fixed point (e.g. point I), one can linearize the system and obtain a linearized Langevin equation. This helps in calculating the correlation coefficients analytically and thus to compare with the numerical results.

Following Eqs. (21) and (22), the volume dependent fixed points of the system are given by

$$x_0 = \frac{c_1}{c_4}, \tag{B.1}$$

$$y_0 = \frac{2c_2c_4}{c_1c_3}\frac{1}{\left(1 - \frac{c_4}{c_1V}\right)}, \tag{B.2}$$

respectively. One can immediately see that the Jacobian at the stationary point is given as

$$\mathbf{A} = \begin{bmatrix} a_1 & a_2 \\ -a_1 - c_4 & -a_2 \end{bmatrix}, \tag{B.3}$$

where $a_1 = \frac{c_2}{\left(1 - \frac{c_4}{c_1V}\right)} - c_4$, and $a_2 = \frac{c_1^2c_3}{2c_4^2}\left(1 - \frac{c_4}{c_1V}\right)$.

If we now evaluate the noise terms at the fixed point, the multiplicative noise terms will be replaced by additive noise terms and the Langevin description of Eqs. (21) and (22) can be written as a multivariate Ornstein–Uhlenbeck process [35]

$$\begin{bmatrix} \dot{x} \\ \dot{y} \end{bmatrix} = \mathbf{A}\begin{bmatrix} x \\ y \end{bmatrix} + \mathbf{B}\begin{bmatrix} \xi_x \\ \xi_y \end{bmatrix}, \tag{B.4}$$

where the $\mathbf{B}$ is given by,

$$\mathbf{B} = \begin{bmatrix} b_1 & b_2 \\ 0 & -b_2 \end{bmatrix}. \tag{B.5}$$

where $b_1 = \sqrt{\frac{2c_1}{V}}$ and $b_2 = \sqrt{\frac{2c_1c_2}{c_4V}}$.

For the coupled Brusselator system, Eq. (B.4) becomes,

$$\begin{bmatrix} \dot{x} \\ \dot{y} \\ \dot{x}' \\ \dot{y}' \end{bmatrix} = \mathbf{A}\begin{bmatrix} x \\ y \\ x' \\ y' \end{bmatrix} + \mathbf{B}\begin{bmatrix} \xi_x \\ \xi_y \\ \xi_c \\ \xi_{x'} \\ \xi_{y'} \end{bmatrix}, \tag{B.6}$$

where the **A** and **B** are now given by,

$$\mathbf{A} = \begin{bmatrix} a_1 - \varepsilon_D & a_2 & \varepsilon_D & 0 \\ -a_1 - c_4 & -a_2 & 0 & 0 \\ \varepsilon_D & 0 & a_1 - \varepsilon_D & a_2 \\ 0 & 0 & -a_1 - c_4 & -a_2 \end{bmatrix}, \tag{B.7}$$

$$\mathbf{B} = \begin{bmatrix} b_1 & b_2 & -b_C & 0 & 0 \\ 0 & -b_2 & 0 & 0 & 0 \\ 0 & 0 & b_C & b_1 & b_2 \\ 0 & 0 & 0 & 0 & -b_2 \end{bmatrix}, \tag{B.8}$$

where $b_C = \sqrt{\frac{2\varepsilon_C c_1}{c_4 V}}$.

Let us define the stationary covariance matrix **C** as

$$\mathbf{C} = \langle \mathbf{x}(\mathbf{t})\mathbf{x}^{\mathbf{T}}(\mathbf{t}) \rangle, \tag{B.9}$$

where $\mathbf{x}(\mathbf{t})$ is given by the column matrix,

$$\mathbf{x}(\mathbf{t}) = \begin{bmatrix} x \\ y \\ x' \\ y' \end{bmatrix} \tag{B.10}$$

Since **A** has eigenvalues with negative real part (the fixed points being stable), the covariance matrix can be solved for the system given by Eq. (B.6) by the following algebraic equation (see Ref. [35, Sec. 4.4.6]):

$$\mathbf{AC} + \mathbf{CA}^T + \mathbf{BB}^T = 0. \tag{B.11}$$

Solving Eq. (B.11) one can obtain C_{xx} and $C_{xx'}$ which gives us the correlation coefficients. Note that the non-square structure of the matrix **B** does not affect Eq. (B.11) because the quantity $\mathbf{BB}^T$ is a square matrix of dimension 4.

References

[1] P.S. Swain, M.B. Elowitz, E.D. Siggia, Proc. Natl. Acad. Sci. USA 99 (2002) 12795.
[2] J. Paulsson, Phys. Life Rev. 2 (2005) 157.
[3] Y. Kuramoto, Chemical Oscillations, Waves, and Turbulence, Springer, Berlin, 1984.
[4] L. Chen, R. Wang, T. Zhou, K. Aihara, Bioinformatics 21 (2005) 2722.
[5] M.B. Elowitz, S. Leibler, Nature 403 (2000) 335.
[6] G. Schmid, P. Hänggi, Math. Biosci. 207 (2007) 235.
[7] T.S. Gardner, C.R. Cantor, J.J. Collins, Nature 403 (2000) 339.
[8] D.T. Gillespie, J. Phys. Chem. 81 (1977) 2340.
[9] N.G. Van Kampen, Stochastic Processes in Physics and Chemistry, North-Holland, Amsterdam, 1992.
[10] D.T. Gillespie, J. Chem. Phys. 113 (2000) 297.
[11] H. Grabert, P. Hänggi, I. Oppenheim, Physica A 117 (1983) 300.
[12] P. Hänggi, H. Grabert, P. Talkner, H. Thomas, Phys. Rev. A 29 (1984) 371.
[13] A. Pikovsky, M. Rosenblum, J. Kurths, Synchronization: A Universal Concept in Nonlinear Science, Cambridge University Press, Cambridge, 2001.
[14] F. Baras, Phys. Rev. Lett. 77 (1996) 1398.
[15] M.E. Taga, B.L. Bassler, Proc. Natl. Acad. Sci. USA 100 (2003) 14549.
[16] D. McMillen, N. Kopell, J. Hasty, J.J. Collins, Proc. Natl. Acad. Sci. USA 22 (2002) 679.
[17] A.F. Taylor, M.R. Tinsley, F. Wang, Z. Huang, K. Showalter, Science 323 (2009) 614.
[18] E. Ullner, J. Buceta, A. Diez-Noguera, J. Garcia-Ojalvo, Biophys. J. 96 (2009) 3573.
[19] P.S. Swain, J. Mol. Biol. 344 (2004) 965.
[20] J. Garcia-Ojalvo, M.B. Elowitz, S.H. Strogatz, Proc. Natl. Acad. Sci. USA 101 (2004) 10955.
[21] M.S. Surette, M.B. Miller, B.L. Bassler, Proc. Natl. Acad. Sci. USA 96 (1999) 1639.
[22] D. Goldobin, A. Pikovsky, Radiophys. Quant. Electron. 47 (2004) 910;
D. Goldobin, A. Pikovsky, Physica A 351 (2005) 126;
D. Goldobin, A. Pikovsky, Phys. Phys. Rev. E 71 (2005) 045201.
[23] H. Nakao, K. Arai, Y. Kawamura, Phys. Rev. Lett. 98 (2007) 184101.
[24] X. Sailer, M. Zaks, L. Schimansky-Geier, Fluctuation Noise Lett. 5 (2005) L299.
[25] R.F. Galán, N. Fourcaud-Trocmé, G. Bard Ermentrout, N.N. Urban, J. Neurosci. 26 (2006) 3646.
[26] J. de la Rocha, B. Doiron, E. Shea-Brown, K. Josić, A. Reyes, Nature 448 (2007) 802.
[27] A. Nandi, G. Santhosh, R.K. Brojen Singh, R. Ramaswamy, Phys. Rev. E 76 (2007) 041136.
[28] I. Prigogine, R. Lefever, J. Chem. Phys. 48 (1968) 1695;
J.J. Tyson, J. Chem. Phys. 58 (1973) 3919.
[29] B. Lindner, J. Garcia-Ojalvo, A. Neiman, L. Schimansky-Geier, Phys. Rep. 392 (2004) 321.
[30] E.I. Volkov, V.A. Romanov, Phys. Scripta 51 (1995) 19.
[31] B. Lindner, L. Schimansky-Geier, Phys. Rev. E 61 (2000) 6103.
[32] Z. Hou, T.J. Xiao, H. Xin, ChemPhysChem 7 (2006) 1520.
[33] G. Schmid, I. Goychuk, P. Hänggi, Europhys. Lett. 56 (2001) 22.
[34] S.H. Strogatz, Nonlinear Dynamics and Chaos: With Applications in Physics, Biology, Chemistry, and Engineering, Perseus Books, Reading, MA, 1994.
[35] C.W. Gardiner, Handbook of Stochastic Processes, Springer-Verlag, Berlin, 1985.